ONLINE DATA SUPPLEMENTARY MATERIAL

Supplementary Methods

Synchronizing the computational algorithm with time-dependent 3-D images:

A sequence of images to capture the beating heart was acquired by high-speed scanning via four steps:

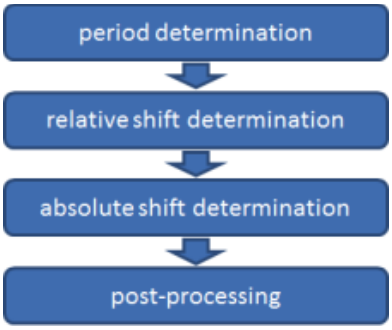

(1) The image sequences to capture a specific section of the heart were split into multiple periods, and the individual periods were processed. Since the Zebrafish heart rates were often not in synchrony with the scanning time, we minimized the difference in the least square intensity with respect to the periodic hypothesis (T) by estimating the period of each sub-sequence.[1, 2] We scanned the fish to ensure that the individual sequence of images cover 4 to 5 cardiac cycles. During post-data processing, the first and last periods were discarded to ensure data integrity. The images capturing the heart at the same instantaneous moment in different periods were correlated. By using this correlation, we adopted the following cost function to estimate the period: $D(z_k, T') = \sum_{m\in Z^2}\sum_{j=1}^{N_\tau-1}\{\left|I_m[x_m, z_k, \tau_{i(j)}] - I_m[x, z_k, \tau_{i(j)}]\right|^2 + \left|\tau'_j - \tau'_{j-1}\right|^2/T'^2\}^{1/2}$ (1), where D denotes the cost function of fitting a period hypothesis, I_m the captured image, τ' the time instance when the image is captured, z_k the z-direction index of a slice, and x_m is a vector denoting the pixel index.

(2) We calculated the relative shift to serve as an indent between image sequences. Despite the identical periods, two image sequences might not be aligned. As mentioned above, the scanning operation proceeded from section to section, and there was an idle time between sections to allow for camera adjustment. When the scanner was ready to capture the next section, the heart was not necessarily in the same cardiac cycle as that of the previous section. The two sections had to be aligned before the 3-D structure reconstruction. This phenomenon was called relative shift determination. Two adjacent sections of the heart should have similar appearances. We exploited this similarity and formulated the relative shift determination in the form of quadratic minimization:[3] $(s) = \int\int_{R^2}\int_0^L |I_m(x, z_k, t) - I_m(x, z_{k'}, t-s)|^2 dtdx$ (2), where $Q_{k,k'}$ denotes a cost function of fitting a relative shift hypothesis, R the possible spatial neighborhood, L the total time of image capturing, and s the relative shift hypothesis.

(3) Next, we converted the relative shift to the absolute shift with respect to the first image sequence. Although relative shift could be used to align two adjacent frames, all of the frames were aligned to reconstruct the entire heart. Upon obtaining all relative shifts, a relation to align the next section given the previous section was built. This recurrent relation was transformed into an absolute relation by solving a linear equation (not shown) using the pseudo-inverse approach as previously described.[4]

Supplementary Tables

Table S1. Coefficients of variation at end-diastole

	Control	Gata1a MO injected	Gata1a MO + Nrg1 mRNA	AG1478 treated
50hpf	15.0%	9.4%	6.7%	12.9%
75hpf	11.5%	12.4%	15.3%	14.2%
100hpf	5.2%	12.7%	6.6%	9.5%

Table S2. Primers for the *in vitro* experiments

Human Hes1:	Forward	TGAGCCAGCTGAAAACACTG
	Backward	GTGCGCACCTCGGTATTAAC
Human Hey1:	Forward	GTTCGGCTCTAGGTTCCATGT
	Backward	CGTCGGCGCTTCTCAATTATTC
Human Jag1	Forward	CAAAGTGTGCCTCAAGGAGTATCAGTCC
	Backward	GAAAGGCAGCACGATGCGGTTG
Human Jag2	Forward	ATGCGACACTCGCTCGAT
	Backward	GTCGTCATCCCCTTCCAGTT
Human Dll1	Forward	CAGGGTTGCACACTTTCTCC
	Backward	GCACGGACCTCAAGTACTCC
Human Dll3	Forward	CCTGCGCGCTGAATGTC
	Backward	CATCGAAACCTGGAGAGAGG
Human Dll4	Forward	CGACAGGTGCAGGTGTAGC
	Backward	TACTTGTGATGAGGGCTGGG

Table S3. Human Nrg1 PCS2+ cloning primers:

hNrg1-Clone	Forward	TCTTTTTGCAGGATCCACCATGGAGATTTATTCCCCAGA CATGTCTG
	Backward	GAGAGGCCTTGAATTCCTATTCAGGCAGAGACAGAAAG GGAGTG

Table S4. Primers for *in vivo* experiments

Zebrafish Jag1	Forward	CCGCGTATGTTTGAAGGAGTATCAGTCG
	Backward	CAGCACGATCCGGGTTTTGTCG
Zebrafish Jag2	Forward	AGCCCTAGCAAAACGAGCGACG
	Backward	GCGTGAATGTGCCGTTCGATCAA
Zebrafish Dll4	Forward	CAAAGTGGGAAGCAGACAGAGCTAAGG
	Backward	CGGTCATCCCTGGGTGTGCATT
Zebrafish BMP10	Forward	GCATCAAGGGGCCACTCGTGTAGA
	Backward	TCGTCTCACTCCACTAGGTCCCATACTG
Zebrafish ErbB2	Forward	GATCAGGACTGCCAAACATTGACGTCT
	Backward	AGCAGCACACTGAACATGGCAGCA
Zebrafish Nrg-1	Forward	GTGTGTTTGTCCCTGTGGACGCGT
	Backward	CCTCCTGGAGCTTCCCCTCAAACA
Zebrafish Notch1b	Forward	CAGAGAGTGGAGGCACAGTGCAATCC
	Backward	GCCGTCCCATTCACACTCTGCATT

Figure S1.

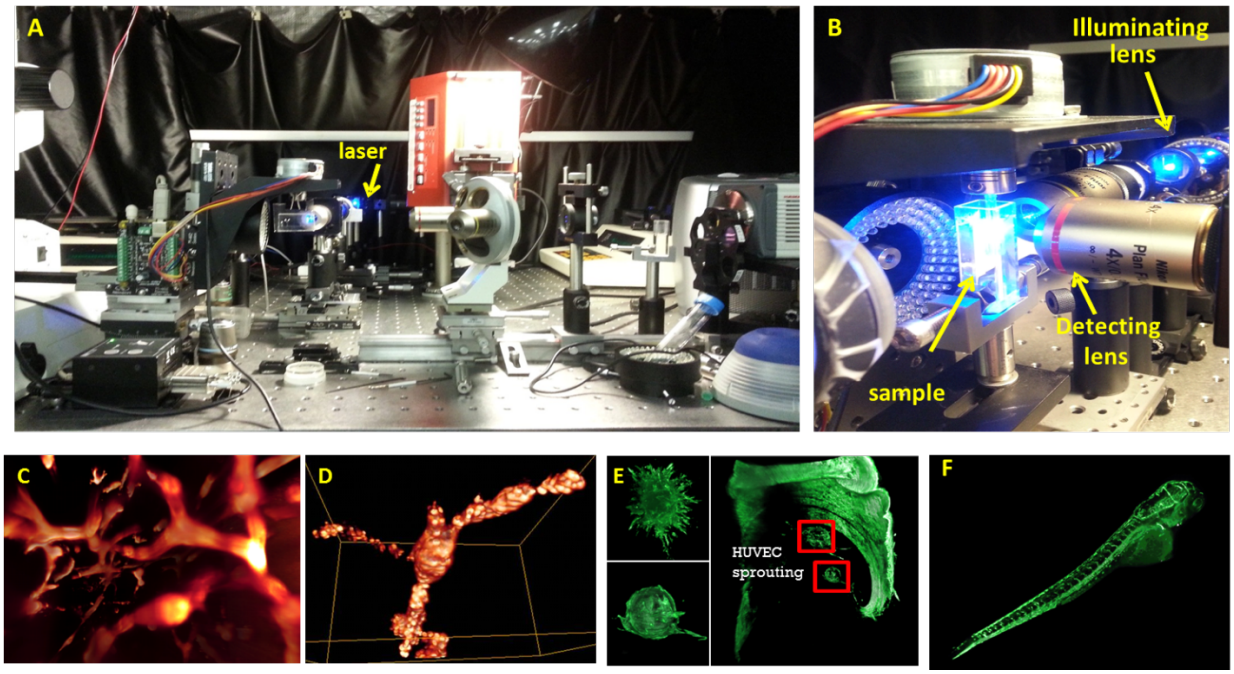
A
laser
B
Illuminating lens
Detecting lens
sample
C
D
E
HUVEC sprouting
F

Figure S2

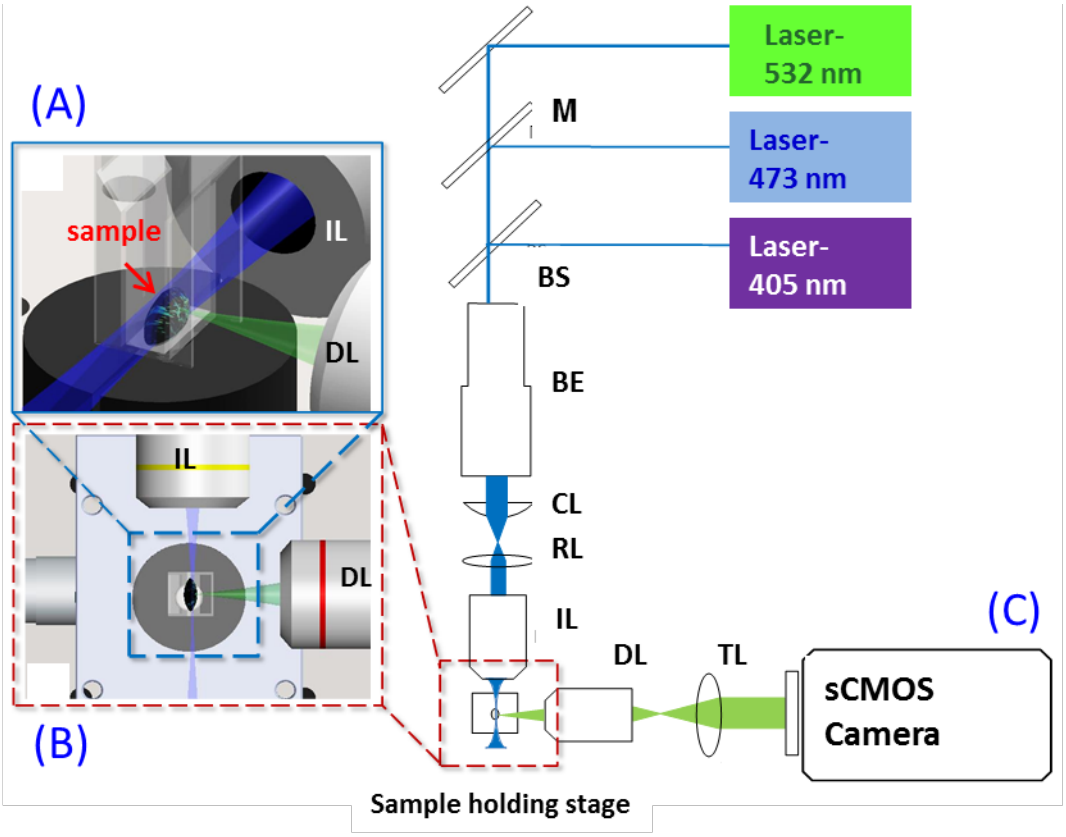
(A)
sample
IL
DL
(B)
IL
DL
Laser-
532 nm
Laser-
473 nm
Laser-
405 nm
M
BS
BE
CL
RL
IL
DL
TL
(C)
sCMOS
Camera
Sample holding stage

Figure S3.

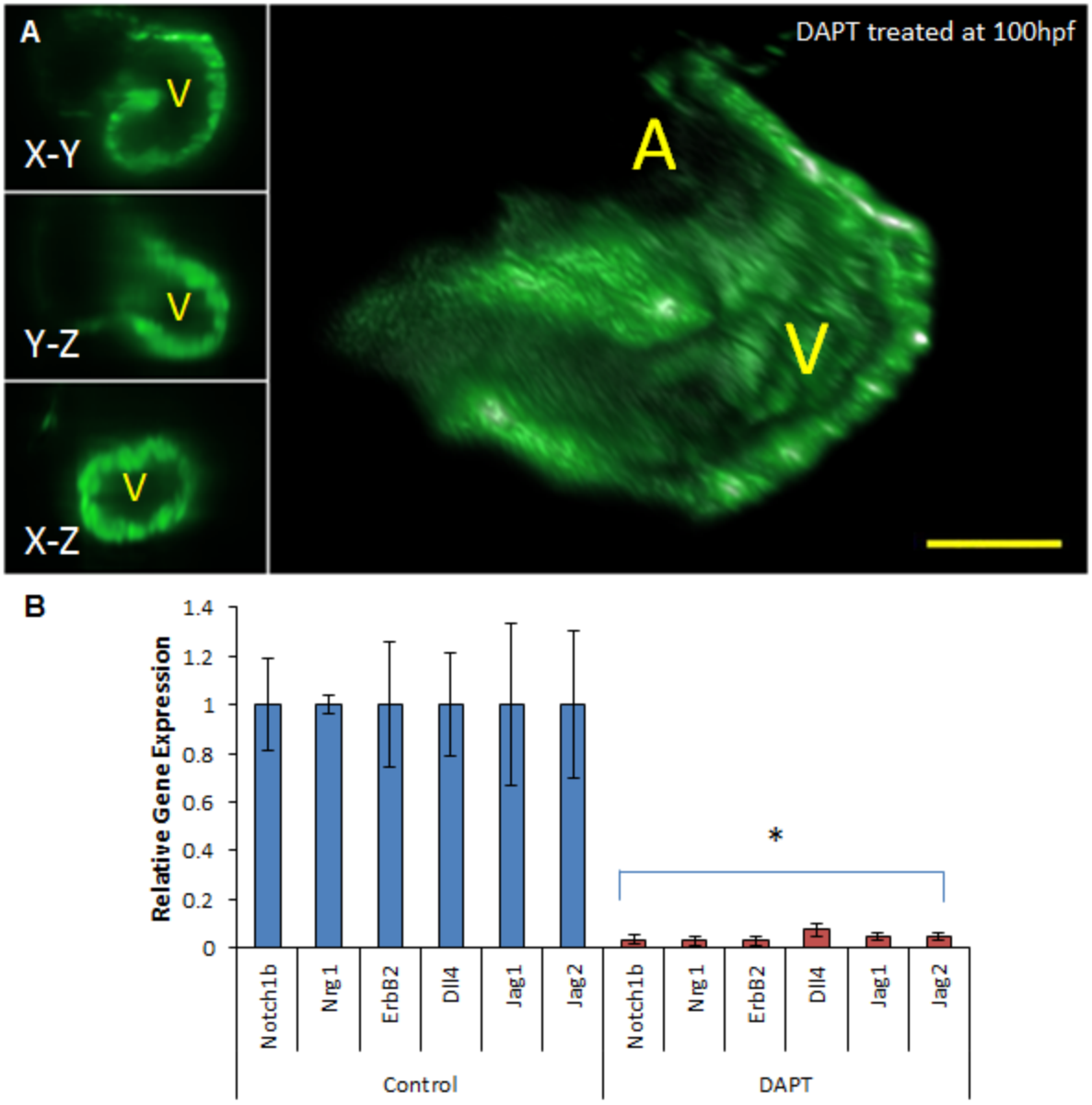
A
V
X-Y
V
Y-Z
V
X-Z
DAPT treated at 100hpf
A
V
B
Relative Gene Expression
1.4
1.2
1
0.8
0.6
0.4
0.2
0
*
Notch1b
Nrg1
ErbB2
Dll4
Jag1
Jag2
Notch1b
Nrg1
ErbB2
Dll4
Jag1
Jag2
Control
DAPT

Figure S4

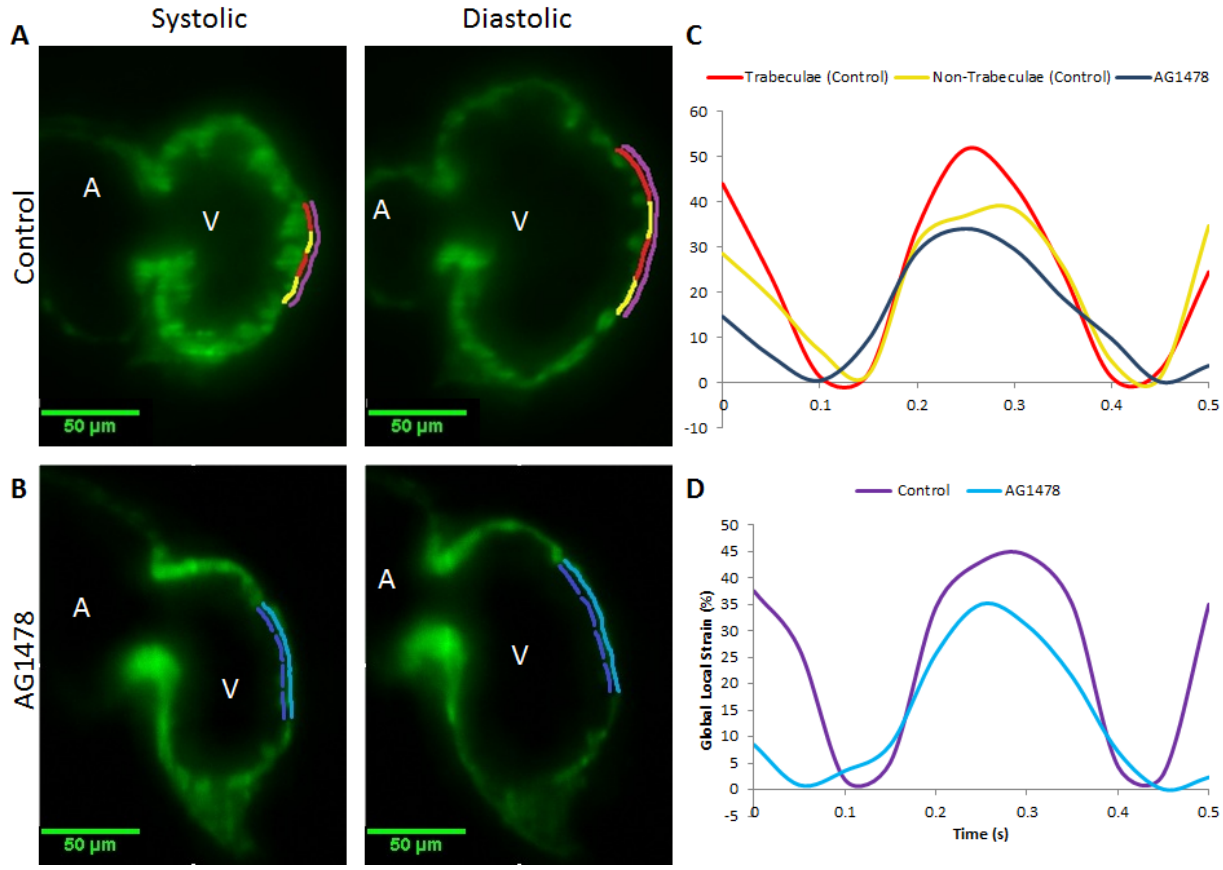
A
Systolic
Diastolic
Control
A
V
50 µm
B
AG1478
C
Trabeculae (Control)
Non-Trabeculae (Control)
AG1478
D
Control
AG1478
Global Local Strain (%)
Time (s)

Figure S5

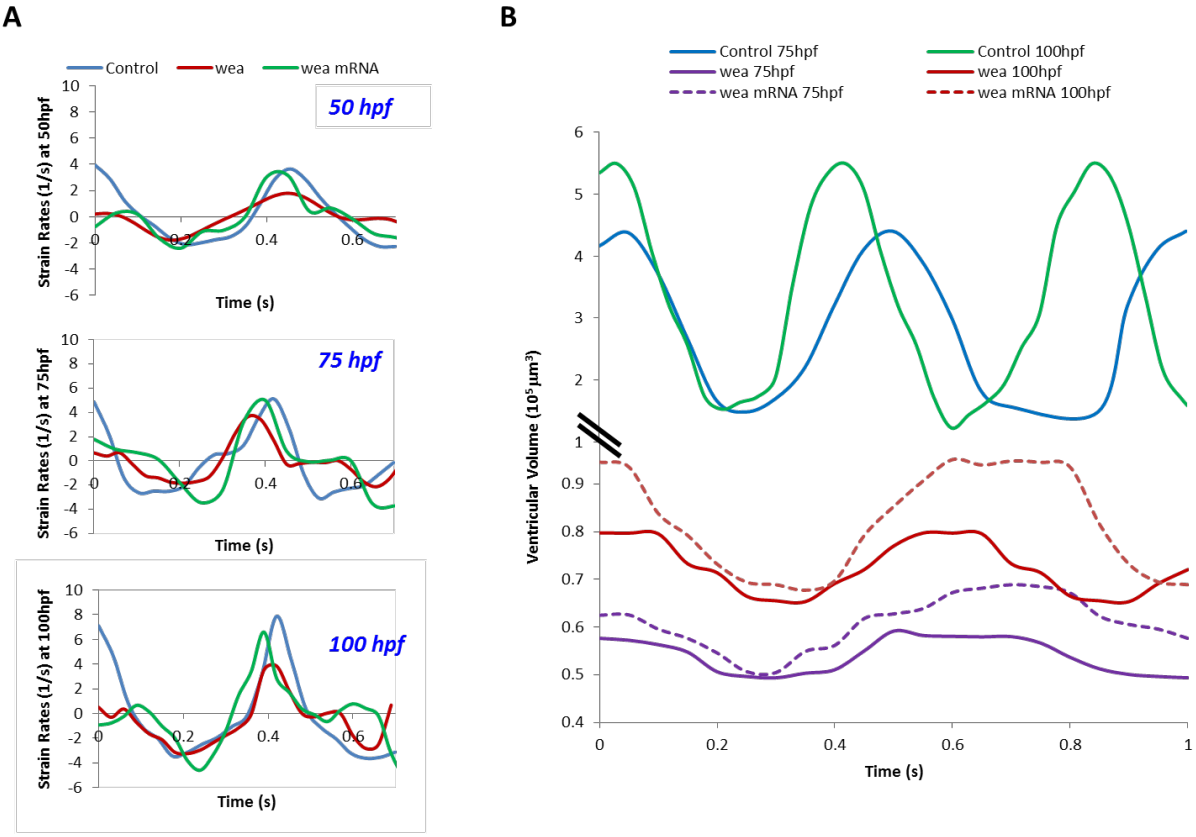
A
Control
wea
wea mRNA
50 hpf
Strain Rates (1/s) at 50hpf
Time (s)
75 hpf
Strain Rates (1/s) at 75hpf
Time (s)
100 hpf
Strain Rates (1/s) at 100hpf
Time (s)
B
Control 75hpf
Control 100hpf
wea 75hpf
wea 100hpf
wea mRNA 75hpf
wea mRNA 100hpf
Ventricular Volume (10⁵ µm³)
Time (s)

Figure S6

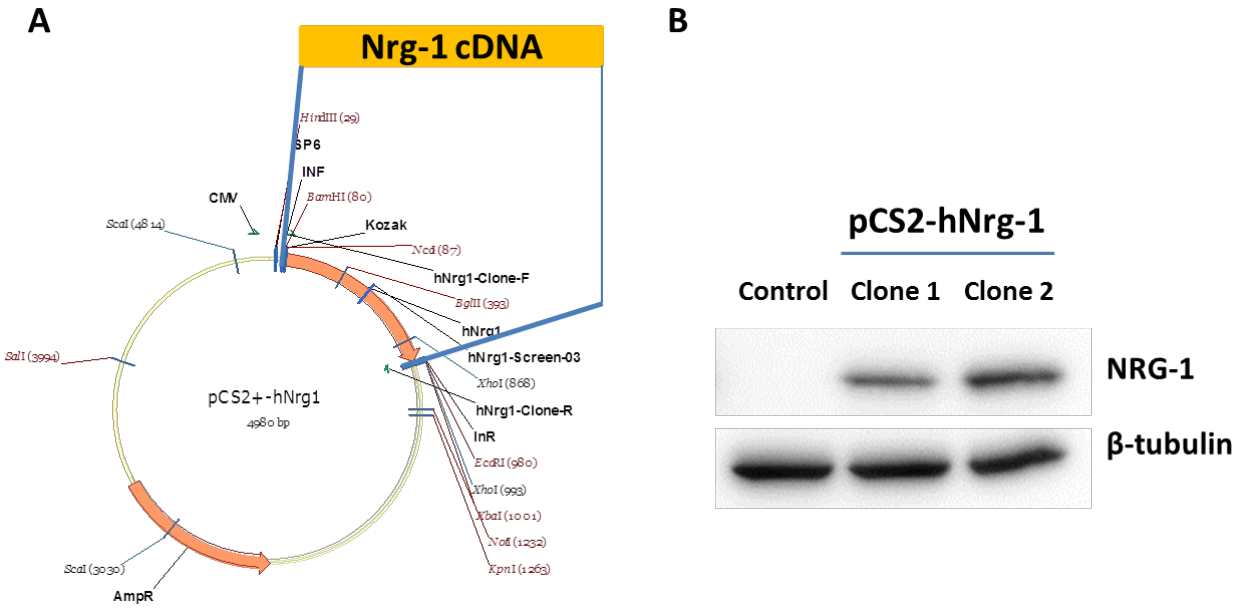
A
Nrg-1 cDNA
HindIII (29)
SP6
INF
BamH1 (80)
Kozak
NcoI (87)
hNrg1-Clone-F
BglII (393)
hNrg1
hNrg1-Screen-03
XhoI (868)
hNrg1-Clone-R
InR
EcoRI (980)
XhoI (993)
XbaI (1001)
NotI (1232)
KpnI (1263)
CMV
ScaI (4814)
SalI (3994)
pCS2+-hNrg1
4980 bp
ScaI (3030)
AmpR
B
pCS2-hNrg-1
Control
Clone 1
Clone 2
NRG-1
β-tubulin

Supplementary Figure Legends.

Figure S1. Our in-house Fluorescent Light-Sheet Microscopy (LSM) and 3-D images. (A) Optical components for the LSM set-up include the laser source(s), illuminating and detecting lenses, and a high-frame rate CMOS camera. (B) A zoomed-in image highlights the sample at the orthogonal intersection between the detecting and illuminating lenses. (C) 3-D LSM images reveal the hepatic cell network at the mm scale, (D) the branching airway at the sub-millimeter scale, (E) the sprouting human umbilical endothelial cells grown in Matrigel, as well as (F) the entire zebrafish embryo imaged at the micron scale.

Figure S2. Schematic diagram of LSM system. Our in-house LSM consists of an illumination and a detection unit. A laser beam (blue line) from one or more lasers is collected and focused by the beam expander to optimize the beam size. A cylindrical lens (CL) converts the laser beam to a sheet of laser light that can transversely illuminate a thin section of sample (A) (B). The sample is mounted at the intersection between illumination lens (IL) and detection lens (DL). The illuminated 2-D thin section (fluorescent detection in green) is captured by the high-frame rate sCMOS camera (C). Note that the illumination axis is orthogonal to the detection axis. The illumination optics is designed to illuminate a very thin volume around the focal plane of the detection objective. M: Mirror, BS: Beam splitter, BE: Beam expander, TL: Tube lens.

Figure S3. γ-secretase inhibitor (DAPT) prevented transmigration of NICD to inhibit Notch signaling and trabeculation. (A) Treatment with DAPT blocked trabeculation. (B) Notch-related mRNA expression was down-regulated in DAPT-treated fish. (t-test, $*p < 0.05$, n=5). A: Atrium, V: Ventricle.

Figure S4. Regional strain measurements. (A) Trabecular (yellow lines) and non-trabecular (red lines) regions from controls as well as their combined myocardial segment (purple lines) are illustrated at end-systole and end-diastole. (B) ErbB signaling inhibitor (AG1478) treatment inhibited trabeculation. Non-trabeculated myocardium (dark blue lines) and the combined myocardial segment (sky blue line) are illustrated at end-systole and end-diastole. (C) Segmental strain curves from trabeculated control regions (red lines), non-trabeculated control regions (yellow lines) and AG1478–treated non-trabeculated regions (dark blue lines) are illustrated. (D)

Comparing the combined strain between controls (purple) and AG1478 treatment (sky blue) illustrates the decrease in contractility in response to AG1478.

Figure S5. Contractile function in response to *wea* mutation. (A) The *wea* mutants developed reduced strain rates when compared to the wild type. Injection of *Nrg1* mRNA moderately restored strain rates. Strain remained at zero during diastole. (B) The *wea* mutants developed a reduced ventricular volume when compared to the wild type. The ventricular contractility (volume change) was partially restored with *Nrg1* mRNA injection at 1-4 cell stage.

Figure S6. Cloning and verification of human *Nrg*-1 (*zNrg*-1) mRNA for zebrafish. (A) Human *Nrg*-1 (*hNrg*-1) cDNA was cloned into pCS2+ vector at the multiple cloning sites. (B) HEK293 cells were transfected with vector alone or two clones from the pCS2-*hNrg*-1 plasmids. Cell lysates were applied to perform the Western blots with anti-*Nrg*-1 antibody. Both pCS2-*hNrg*-1 clones expressed *Nrg*-1 protein at the anticipated band size.

Supplementary Video Legends

Video S1. Control heart scan

Video S2. *Gata1a* MO heart scan

Video S3. Rescued by *Nrg-1*

Video S4. *Tnnt2a* MO heart scan

Video S5. *Cloche* mutant heart scan

Video S6. Blood circulation from control zebrafish

Video S7. Blood circulation from *EPO* mRNA injected zerbafish

Video S8. 4-D beating zebrafish heart image

Supplemental References

1. Dworetsky M. A period-finding method for sparse randomly spaced observations or "how long is a piece of string?". *Monthly Notices of the Royal Astronomical Society*. 1983;203:917-924
2. Stellingwerf R. Period determination using phase dispersion minimization. *The Astrophysical Journal*. 1978;224:953-960
3. Thevenaz P, Ruttimann UE, Unser M. A pyramid approach to subpixel registration based on intensity. *Image Processing, IEEE Transactions on*. 1998;7:27-41
4. Liebling M, Forouhar AS, Gharib M, Fraser SE, Dickinson ME. Four-dimensional cardiac imaging in living embryos via postacquisition synchronization of nongated slice sequences. *Journal of biomedical optics*. 2005;10:054001